JOURNAL OF SPACECRAFT AND ROCKETS
Vol. 38, No. 4, July–August 2001

Infrared Sensing Aeroheating Flight Experiment: STS-96 Flight Results

Robert C. Blanchard,* Richard G. Wilmoth,† Christopher E. Glass,† N. Ronald Merski Jr.,* and Scott A. Berry‡
NASA Langley Research Center, Hampton, Virginia 23681-2199
Timothy J. Bozung§
George Washington University, Hampton, Virginia 23681-2199
and
Alan Tietjen,¶ Jodean Wendt,** and Donald Dawson††
Computer Sciences Corporation, Kennedy Space Center, Florida 32899-0001

Major elements of an experiment called the infrared sensing aeroheating flight experiment are discussed. The primary experimental goal is to provide reentry global temperature images from infrared measurements. These measurements are used to define the characteristics of hypersonic boundary-layer transition during flight. Specifically, the experiment is to identify, monitor, and quantify hypersonic boundary-layer windward surface transition of the X-33 vehicle during flight. In addition, the flight data will serve as a calibration and validation of current boundary-layer transition prediction techniques; provide benchmark laminar, transitional, and fully turbulent global aeroheating data to validate existing wind-tunnel and computational results; and advance aeroheating technology. Shuttle Orbiter data from STS-96 are used to validate the data acquisition, and data reduction to global temperatures, to mitigate the experiment risks before the maiden flight of the X-33, is discussed. STS-96 reentry midwave (3–5 μm) infrared data were collected at the Ballistic Missile Defense Organization/Innovative Sciences and Technology Experimentation Facility site at NASA Kennedy Space Center and subsequently mapped into global temperature contours using ground calibrations only. A series of image mapping techniques have been developed to compare each frame of infrared data with thermocouple data collected during the flight. Comparisons of the ground calibrated global temperature images with the corresponding thermocouple data are discussed. The differences are shown to be generally less than about 5%, which is comparable to the expected accuracy of both types of aeroheating measurements.

Nomenclature

B_{set}	=	calibration offset values obtained during system setup
C_2	=	constant in Planck's equation
c	=	speed of light
G_{set}	=	calibration gain values obtained during system setup
h	=	altitude
$\hbar$	=	Planck's constant
k	=	Boltzman's constant
$L_{\text{BB}}(T)$	=	surface squareband blackbody radiance
L_m	=	blackbody spectral radiance
L_p	=	apparent radiance at focal plane
L_{path}	=	atmosphere band radiance
M	=	Mach number
M_e	=	boundary-layer edge Mach number
R	=	detector response (counts)
Re_L	=	Reynolds number per unit length
Re_θ	=	momentum thickness Reynolds number
T	=	surface temperature
T_C	=	thermocouple temperature
T_{IR}	=	infrared temperature
α	=	angle of attack
β	=	side slip angle
$\varepsilon(T)$	=	surface emissivity
λ	=	wavelength
τ_{atm}	=	path transmittance
ϕ	=	roll angle

Received 20 September 2000; revision received 6 February 2001; accepted for publication 3 March 2001.

*Aerospace Engineer, Aerothermodynamics Branch, Aerodynamics, Aerothermodynamics, and Acoustics Competency. Associate Fellow AIAA.

†Aerospace Engineer, Aerothermodynamics Branch, Aerodynamics, Aerothermodynamics, and Acoustics Competency. Senior Member AIAA.

‡Aerospace Engineer, Aerothermodynamics Branch, Aerodynamics, Aerothermodynamics, and Acoustics Competency.

§Graduate Research Scholar Assistant, Joint Institute for Advancement of Flight Sciences. Member AIAA.

¶Senior Research Scientist, Ballistic Missile Defense Organization/Innovative Sciences and Technology Experimentation Facility. Member AIAA.

**Engineer, Ballistic Missile Defense Organization/Innovative Sciences and Technology Experimentation Facility.

††Research Scientist, Ballistic Missile Defense Organization/Innovative Sciences and Technology Experimentation Facility.

Introduction

ATMOSPHERIC reentry boundary-layer transition, corresponding to a sudden increased surface heating associated with the vehicle boundary layer going from laminar to turbulent flow, has been demonstrated in both flight data and wind-tunnel testing. This heating phenomenon can impact thermal protection system (TPS) material selection, split-line location, and material thickness, which results in a prominent weight impact and presents challenges for future reusable launch vehicles (RLVs). The increased heating to the vehicle surface is significant when transition takes place because increases of a factor of two or more in heating level occur on the windward surface of the vehicle. Boundary-layer transition occurs naturally as a reentry vehicle descends to higher densities, corresponding to increased Reynolds number, and its occurrence has been well demonstrated with smooth models in wind tunnels for many years.[1] As observed for the Shuttle Orbiter, transition can occur early in the entry trajectory due to roughness factors.[2] Thus, one design goal for the TPS is to constrain the vehicle surface roughness in an attempt to avoid early transition. Also, there are typically flight operation impacts such as flight-to-flight inspections and maintenance to reduce the risk of early transition. Progression to a full RLV requires that the boundary-layer transition effects be well understood and taken into account in any RLV design.

Correlation parameters have been formulated to approximate conditions at which boundary-layer transition will occur in flight. For

example, the incipient, critical, and effective roughness Reynolds numbers have been used in the heating analysis of the first flights of the Shuttle Orbiter.[3] The correlation parameters are semi-empirical insofar as transition criteria are dependent on design factors that are developed through wind-tunnel or flight experiments, or a combination of both. Also, there is the micro- and macrosurface dependency (i.e., forward surface protuberances can trigger early transition), whereas other material surface properties need to be taken into account for the actual flight vehicle, particularly surfaces that are sensitive to thermal expansion.

The correlation factor used to estimate flight boundary-layer transition for the X-33 is Re_θ divided by M_e (Ref. 4). This correlation factor for the X-33 metallic TPS has been developed in a synergistic approach between computational fluid dynamics (CFD) and wind-tunnel tests. It is important to verify this correlation with the flight vehicle, and although the X-33 is equipped with arrays of surface thermocouples, global information is required for a definitive observation of the complex boundary-layer transition. Accordingly, an infrared imaging experiment has been devised to provide global temperature images to define the character of the transition period during flight. The experiment is called the infrared sensing aeroheating flight experiment (ISAFE) and is discussed in this report. (Some nontechnical experiment details are also found in proposal NRA 8-21, "Flight Technologies for Reusable Launch Vehicles," NASA Langley Research Center, 3 April 1998.) In addition, the ISAFE methodology is being developed as a general versatile tool to provide flight global heating data for reentry vehicles at hypervelocity speeds.

Four main areas of work are required for the successful accomplishment of ISAFE. These areas are 1) site selection, that is, where to put the portable optical mounts; 2) data acquisition, that is, target acquisition, tracking, and data recording; 3) data reduction to global temperature–time histories; and 4) comparison of the flight results to theory, wind-tunnel data, and/or CFD simulations. The Shuttle Orbiter was chosen as a flight target to minimize the experiment risks of acquiring useful flight data before the maiden flight of the X-33. The Orbiter has many of the elements needed to check out the software and data reduction techniques required to produce global surface temperatures, including onboard surface thermocouples. For the initial ISAFE checkout, it was decided to concentrate on areas 2 and 3 by keeping the optical mounts at the Ballistic Missile Defense Organization/Innovative Sciences and Technology Experimentation Facility (BMDO/ISTEF) site at NASA Kennedy Space Center (KSC). This report presents a discussion of the ISAFE and presents the data acquired, as well as the analysis of the flight data on the STS-96 Orbiter reentry.

Experiment Objectives

The objective of the ISAFE is to identify, monitor, and quantify hypersonic boundary-layer transition for the X-33 vehicle during flight. The objectives include, specifically, the global mapping of the transition movement over the windward surface. The data collected during flight will serve as a calibration and validation of current boundary-layer transition prediction techniques. In addition, the flight experiment goal is to provide benchmark laminar, transitional, and fully turbulent global aeroheating data to validate existing full-scale wind-tunnel predication methodology[5] and computational results[6] and to advance aeroheating technology.

Experiment Approach

Trajectory Considerations

The experimental technical approach is to collect global windward surface temperature data with ground-based infrared emission cameras as the X-33 descends through the upper atmosphere. The primary emphasis will be to view the X-33 during both the peak heating portion of the trajectory and the region of expected boundary-layer transition. Figure 1 is a time history graph of several trajectory parameters, namely, Mach number, altitude ($\times 10^3$ feet), and angle of attack (degrees), for a typical X-33 trajectory emanating from Edwards Air Force Base, California and landing at Michael Air Force Base, Utah. The approximate regions where boundary-layer transition is expected, during both ascent and descent, based on the correlation factor (Re_θ/M_e) discussed earlier, are shown to occur between Mach numbers 8 and 10, corresponding to an altitude between 150 and 180 kft. These distances are the minimum viewing requirement for a ground-based camera. However, because the angle of attack is high in the region of expected transition, optimum viewing of the windward surface may be obtained by placing the mobile mounts forward of the trajectory ground track even though the slant range is larger than the minimum distance. Coverage of the X-33 surface requires a combined telescope and infrared detector system having adequate resolution for these distances.

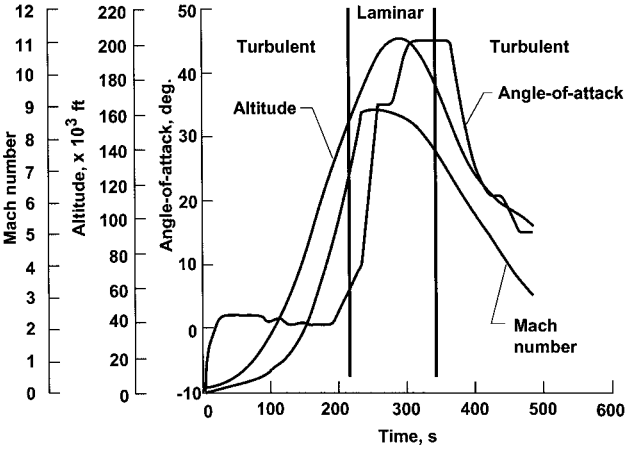

Fig. 1 Typical X-33 trajectory parameters for Michael Air Force Base landing.

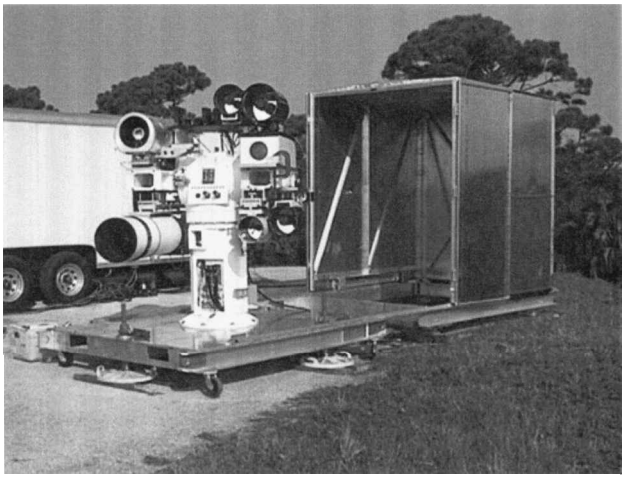

Fig. 2 Typical BMDO/ISTEF mobile optical tracking mount [Small Transportable ISTEF Pedestal System (STRIPS) Mount].

Portable Optical Systems

The measurements will be accomplished nonintrusively (no impact on vehicle airframe or operations) using ground-based optical instruments of the BMDO/ISTEF. The equipment consists of portable optical tracking mounts, which can be equipped with a variety of telescopes (up to 30-in. apertures), and a variety of detectors ranging in wavelength from ultraviolet to the midband infrared, which includes the visible. Figure 2 shows a typical telescope configuration for one of the several tracking mounts in operation at the BMDO facility.

The 24-in. telescope shown at the lower left of the mount can be instrumented with a midwave infrared detector to conduct this experiment. The other telescopes can be fitted with other wavelength sensitive detectors, for example, long-wave infrared, so that simultaneous multiple wavelength data can be collected. Using multiple wavelengths has certain advantages to minimizing the atmospheric effects. The mount control system, communications equipment, and data acquisition systems are contained in a mobile trailer (in background), which completes the data collection and tracking system. Extensive software and communication links have been developed

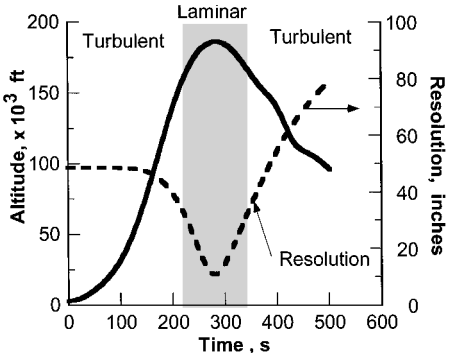

Fig. 3 Altitude and approximate image pixel resolution of simulated X-33 images.

for optimally acquiring, tracking, collecting, and reducing flight data.

Tracking Mount Positioning

The optical tracking mount(s) will be strategically positioned very nearly under the planned ground track of the X-33 to capture the aeroheating data during flight. A typical X-33 ground track launched from Edwards Air Force Base and landing at Michael Air Force Base flies over the Nevada desert when transition is likely to occur. For illustration purposes, the tracking mobile system is assumed to be directly under the ground track where the X-33 achieves maximum altitude. This location corresponds to a position northwest of Las Vegas.

Simulated optical data were generated at this location to provide thermal map sequences for the typical trajectory shown on Fig. 1 to determine experiment feasibility for the highest altitude. Using the telescope properties and the resolution of the sensor charge-coupled device (CCD) (512×512 pixels) provided some assurance that a global thermal image is within the capability of the BMDO/ISTEF portable imaging systems. Figure 3 shows a time history of altitude ($\times 10^3$ feet) and the corresponding approximate image pixel resolution for the simulation. In the region of peak altitude the resolution is about 12 in. for a 60^+-ft vehicle. This resolution corresponds to about three pixels to every two TPS tiles, on the average, roughly equivalent to three thermocouples per two tiles, which should be sufficient to characterize peak heating behavior. For this particular simulation, the resolution is about 30 in. during boundary-layer transition, which provides less than optimal coverage. However, through optimization of the optical mount location, or application of multiple mounts, resolution during transition can be significantly improved. Other factors, such as atmospheric effects, will need to be taken into account in selecting the final mount location(s).

Infrared radiance images are collected at 30 frames/s and will be reduced to surface temperature using calibration factors discussed subsequently. Infrared radiance data are recorded, typically as 12-bit digital data and analog RS-170 video output. Discrete onboard surface temperature measurements will be compared with calibrated ground-based infrared measurements to enhance credibility of quantitative temperature values. Also, postflight assessments will be performed using wind-tunnel data and CFD codes.

Shuttle Flight Data

Shuttle Orbiter flights were selected as targets of opportunity to demonstrate the capability of the ground-based infrared equipment and the data reduction techniques, to mitigate the aeroheating experiment risks before the maiden flight of the X-33. The shuttle serves as an ideal target to provide data for development of measurement and processing techniques because there is a vast aeroheating database that currently exists, particularly on boundary-layer transition. In addition, shuttle aeroheating flight data are collected during each reentry using surface thermocouples.

The initial shuttle data collection has been specifically selected to validate only selected elements of the experiment, namely, the data acquisition processes (i.e., target acquisition, tracking, and data recording) and the data reduction process of reducing infrared images to global surface temperature. Subsequent shuttle data acquisitions are planned to validate the remaining elements of the ISAFE, such as developing a mount position strategy and imaging the shuttle during boundary-layer transition.

STS-96 Data Acquisition

Infrared imagery was collected during the STS-96 landing at NASA KSC, Florida, on 6 June 1999. Figure 4 shows the ground track of the STS-96 as it approaches the landing strip at NASA KSC. The segment of the ground track where infrared data were acquired and the location of the BMDO/ISTEF tracking site are shown. Image data were acquired just before the heading alignment circle when the astronauts take control of the approach and land the vehicle. For this flight, the Orbiter entered on orbit number 153, which is earlier than nominal. Data were acquired directly south of the site after a sky search. On initial image acquisition, the automatic tracking system successfully tracked the Orbiter until it flew almost directly over the site and the telescope gimbals were not able to keep up with the shuttle's motion across the sky. For the shuttle, unlike X-33, optimal placing of ground-based camera systems is difficult due to deorbit go/nogo options exercised only minutes before deorbit, which can significantly change the ground track. Although the shuttle is difficult to acquire in the sky due to last minute trajectory changes, which impact the viewing from the preflight selected mount position, the target acquisition, tracking, and data recording systems used for the shuttle will be similar to the X-33 mission.

Figure 5 shows the Orbiter's Mach number and the corresponding altitude as it approached the landing runway at NASA KSC. These graphs are generated from the postflight trajectory provided by the Orbiter project office at NASA Johnson Space Center (JSC). Also shown on the graphs is the segment of infrared image acquisition. As seen, the initial data acquisition altitude is about 70,000 ft; however, the slant range was about 101,000 ft with the elevation angle about 46 deg above the horizon. When the Orbiter flew over the site the altitude was about 60,000 ft, which closely corresponds to the slant range. During acquisition, the Mach number varied from about 1.95, soon after the pressure probe deployed, which acquires

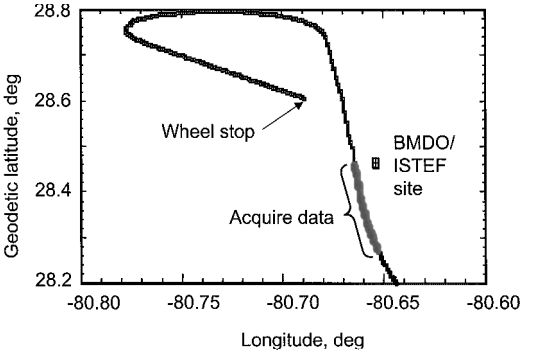

Fig. 4 STS-96 landing approach ground track with data acquisition segment.

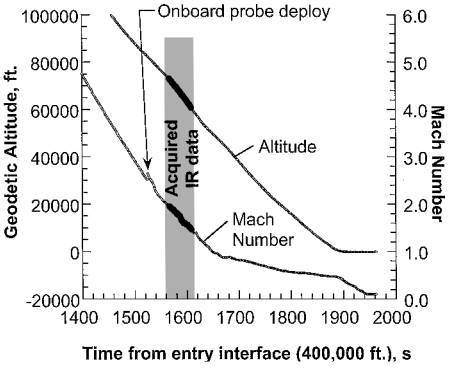

Fig. 5 STS-96 geodetic altitude and Mach number near landing at NASA KSC.

data for onboard Mach number calculations, down to about 1.48. At these conditions, the windward surface of the Orbiter residual heat from the earlier high-heating reentry phase was sufficient for infrared measurements. The shuttle data interval does not encompass the planned X-33 high-altitude data interval. For the initial experiment development, the objectives are to concentrate on data acquisition and data reduction rather than acquisition of data specific to boundary-layer transition.

The orientation of the Orbiter as it approaches landing at NASA KSC is given in Fig. 6. These graphs were generated from postflight trajectory data obtained from the Orbiter project office at NASA JSC. During infrared (IR) imaging, labeled acquire IR data on the graph, the side slip angle is nearly constant at about −1.0 deg, whereas the angle of attack and roll angles both start out at about 10 deg, with the roll angle approaching 0 deg and the angle of attack reducing slightly by the end of the data acquisition.

STS-96 Thermocouple Data

On each Orbiter reentry, limited thermocouple data are collected for purposes of diagnostics after the flight. Figure 7 presents the windward surface thermocouple flight data acquired during the STS-96 reentry. The reference time on each graph is from entry interface (400,000 ft) and the locations of the thermocouples on the bottom surface of the Orbiter are shown. The three digits on each graph represent the last three digits of the measurement system identification (MSID), NASA JSC flight data identification nomenclature. The graphs show the temperature rise during boundary-layer transition from laminar to turbulent in the vicinity of 1200 s after entry interface. The rise in temperature is relatively quick, on the order of tens of seconds. Also, when the times of the temperature pulse peak for the different thermocouples are noted, it is observed that transition occurs first near the rear of the body (on the body flap) and moves forward on the Shuttle Orbiter with time.

Figure 7 shows the measured change in temperature and the transient behavior of the boundary-layer transition on the windward surface, a major element of subsequent ISAFE validation tests. In contrast, the thermocouple data corresponding to the time interval when the IR data were acquired are given in Fig. 8. Shown are the centerline thermocouple measurements, which, when the IR data were acquired, ranged between about 325 and 175°F . Adding the remaining thermocouple measurements does not provide more insight because the surface is nearly uniform in temperature during the IR measurements.

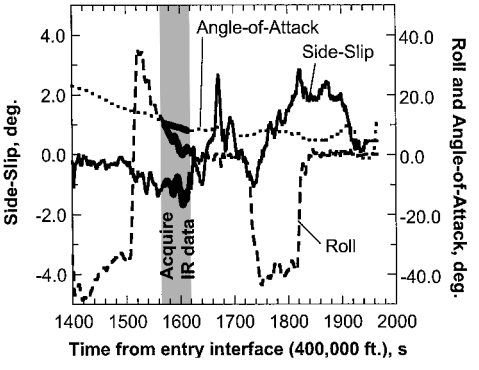

Fig. 6 STS-96 body axis orientation near landing at NASA KSC.

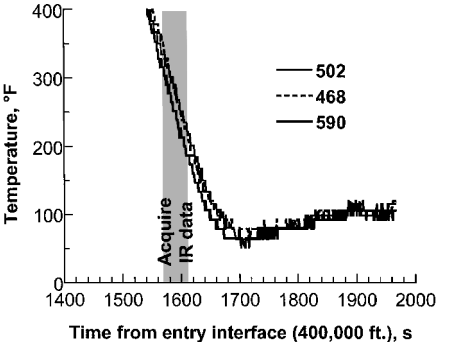

Fig. 8 STS-96 centerline windward thermocouple data (expanded scale).

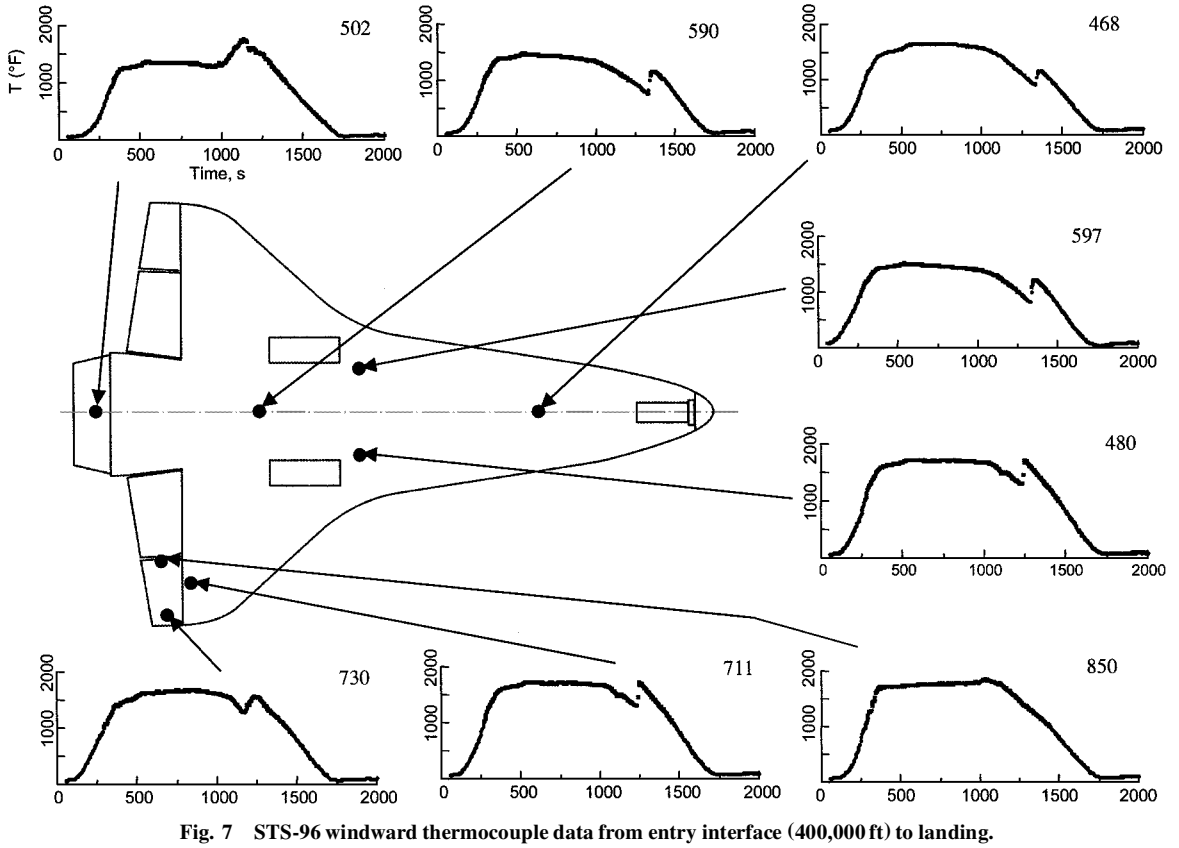

Fig. 7 STS-96 windward thermocouple data from entry interface (400,000 ft) to landing.

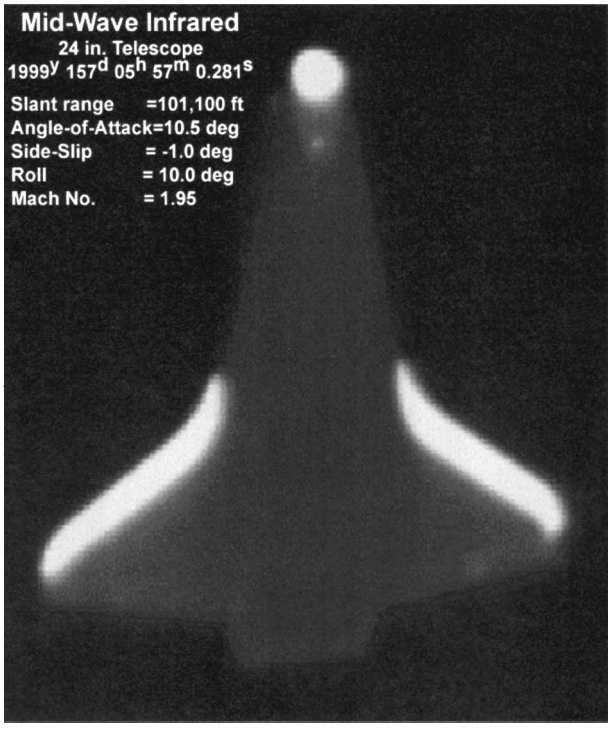

Fig. 9 IR image of STS-96 during reentry.

Table 1 Error estimate for BMDO/ISTEF MWIR 24-in. imaging system

Error source	For setup 1, %	For setup 2, %
Atmosphere self radiance and attenuation	5.0	5.0
Blackbody uncertainty (includes emissivity, temperature, and uniformity uncertainty)	2.5	2.5
System noise estimate (derived from standard deviation of uniform source under observation, worst case)	7.1	10.2
Least-square linear error estimate (mean difference of known source data points)	14.0	3.4
Root sum square error	16.7	12.1

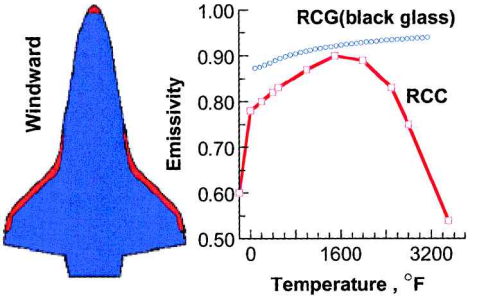

Fig. 10 Orbiter windward surface emissivity as a function of temperature (from NASA Ames Research Center).

STS-96 IR Radiance Data

Two sets of midwave (3–5 μm) IR data were collected during STS-96 reentry, one using the 24-in. aperture telescope and a separate set of data using the 12.5-in. aperture telescope. Over 1260 images from each sensor were collected. Attempts were made to acquire images using the long-wave IR (LWIR) detector (8–12 μm), but a malfunction of the accompanying controller prevented its use. Also, the 12-bit digital system encountered problems so that the data collected were confined to 8-bit analog. Figure 9 shows a typical IR image taken early in the data acquisition time period. The bright areas in the image correspond to hotter surfaces when compared to darker areas (assuming constant surface emissivity). For the image shown, this is approximately true because the emissivity of the reinforced carbon/carbon (RCC) wing leading edges (and nose cap) and the reacting cured glass (RCG, black glass) tiles over most of the windward surface are nearly equal for the temperatures of the Orbiter during this time. The detector settings were optimized for the bottom surface of the Orbiter (i.e., maximum temperature resolution) with the consequence that the RCC leading edges were in saturation for the measurements. The extra bright wing leading edge and the nose cap in Fig. 9 are in detector saturation, which, for the setting used for this image, corresponds to temperatures in excess of 550°F. (The other detector setting used during the flight saturated at about 800°F.) The temperatures deduced from this and subsequent radiance IR image show the leading edge as warm areas (as expected) and a fairly benign (approximately uniform) windward heating. The transformation of the radiance images to temperature is discussed next.

STS-96 IR Temperature Data

The transformation of the radiance IR data to surface temperature depends on several factors, including vehicle surface emissivity, path transmittance, atmospheric radiance, optics radiance, and other calibration factors from a bench and field calibration obtained during setup of the telescope/detector system before flight.

The method used to obtain the surface temperature is to develop a lookup table of the detector response (in count units) as a function of surface temperature using the following equation:

$$R = G_{\text{set}} L_p(T) + B_{\text{set}} \tag{1}$$

where

$$L_p(T) = L_{\text{BB}}(T)\varepsilon(T)\tau_{\text{atm}} + L_{\text{path}}$$

The surface emissivity of the Orbiter has been obtained from NASA Ames Research Center and is shown in Fig. 10 (data contained in a computer database, URL: http://asm.arc.nasa.gov, TPSX WEB V2, "Thermal Protection System Expert and Materials Properties"). For the calculations of temperature, the RCG emissivity values were used because the RCC surface was in saturation. Note, however, that at the surface temperatures of the images (between 175–325°F) that the emissivity differs by only about 10%. It is also assumed for this analysis that the surface emissivity has no wavelength dependence.

The atmospheric path transmittance τ_{atm} and the atmospheric radiance L_{path} have been calculated using the atmosphere model program MODTRAN.[7] Local meteorology soundings and measurements obtained from Patrick Air Force Base during the time of STS-96 reentry were used as inputs to the program to obtain as realistic estimates as possible. Two other verification checks were performed on the MODTRAN output. These are the sky background (i.e., a measurement of the background sky at various telescope elevations without the target), and by using a calibrated stellar source, Alpha Bootis.[8] Both input sources were within expected radiance errors of about 5% for each setup (Table 1). The resulting MODTRAN data used in the extraction of temperature are given in Figs. 11a and 11b, which show the path transmittance and the atmospheric radiance as a function of time from entry interface. The time interval shown includes the interval in which the IR data were acquired.

Two calibrations are performed and used to interpret the flight IR images, a bench calibration and a field calibration. The bench calibration establishes the initial relationship between the irradiance and the sensor output. This is accomplished in the laboratory with a calibrated blackbody source. A temperature is selected for the blackbody, and the sensor output is analyzed for average intensity and standard deviation. When this procedure for various temperatures over the dynamic range for the selected setup is repeated, an incidence radiance and sensor output relationship can be found in the form of a linear equation. The other calibration is the field calibration, which consists of placing a calibrated blackbody source beyond the minimum distance the telescope can

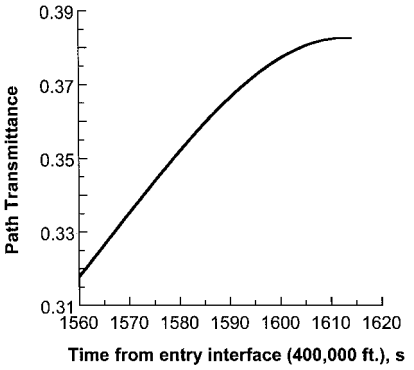

a) Path transmittance time history

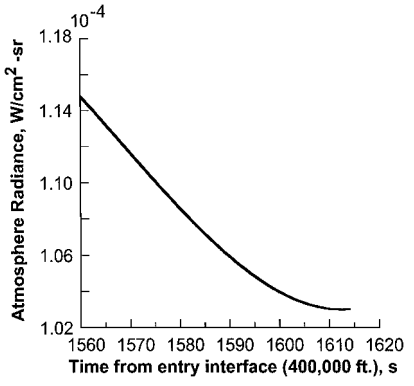

b) Atmosphere radiance time history

Fig. 11 Atmosphere path transmittance and radiance during STS-96 IR data acquisition using MODTRAN.

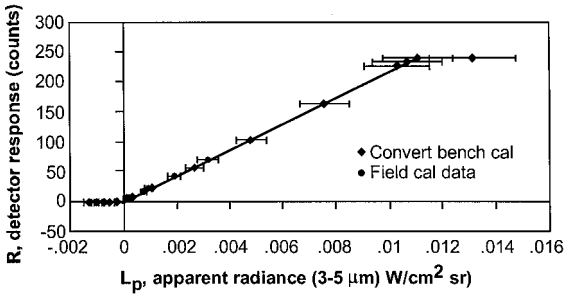

Fig. 12 BMDO/ISTEF 24-in. telescope, MWIR detector, system response (for setup 2).

focus in the field. This calibrates the system as a whole, including the optics. Using several interim setup procedures results in a complete transfer function that combines the effects of the sensor, the optics (including filters), and the recording device(s). The calibration curve resulting from these calibrations for setup 2, the 24-in. aperture telescope, and the midwave IR (MWIR) (3–5 μm) detector is given in Fig. 12. The system output (counts) can be transformed to apparent radiance of the vehicle by application of this curve (apparent here means the effects of the atmosphere have not been fully taken into account). Included in Fig. 12 are error bar estimates at each of the calibration points. This is one of two calibration curves used in the STS-96 data reduction and interpretation process.

Applying the elements discussed earlier to the 1200$^+$ frames of radiance data collected on STS-96 results in a corresponding global temperature for each frame. A typical example of one of the frames is given in Fig. 13, which shows the surface temperature (degrees Fahrenheit) as a spectrum of colors ranging from blue (cool) to red (hot), as noted on the side of the image. The results are preliminary in nature in that directional surface emissivity and possibly low-resolution effects have not been accounted for (resulting in the apparent drop in temperature around the wing leading edges).

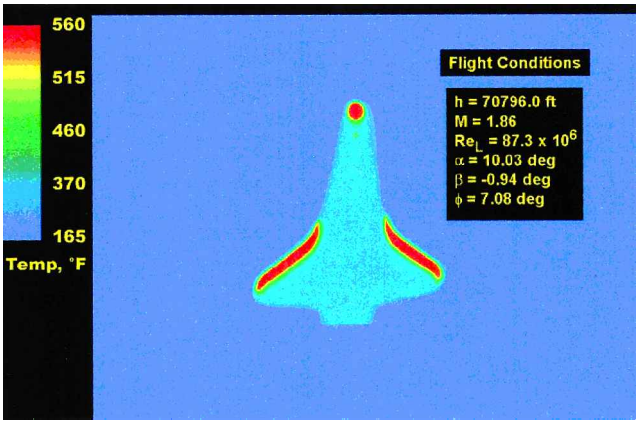

Fig. 13 STS-96 global temperature data from ground calibrated IR observations.

Uncertainty Estimates

The errors associated with the radiance measurements contain several elements and are setup dependent. Table 1 provides the error sources as well as estimates of their contribution to the overall uncertainty. The radiance errors shown are considered worst case and are not uniform over the measurement range as can be observed, for instance, from the error bars in Fig. 12. To obtain a corresponding approximate error in the temperature, consider the relative error relationship between temperature and radiance, namely,

$$\frac{\delta T}{T} = \frac{(e^{C_2/T} - 1)T}{e^{C_2/T} C_2} \frac{(\delta L_m)}{L_m} \tag{2}$$

where

$$C_2 = \hbar c/\lambda k \tag{3}$$

For the temperatures encountered during STS-96 and the measurement wavelengths, the estimate of temperature error for the radiance errors shown is less than 2%, which shows that a large uncertainty in radiance does not necessarily produce a large error in temperature.

Thermocouple and IR Temperature Comparisons

A four-step image reconstruction methodology for associating IR image pixels with thermocouple locations was developed using image processing and simplified photogrammetry theory.[9] The approach has been made general enough to allow for automated processing of the large number of images acquired in this study. First, for a given frame, a projection of the three-dimensional Orbiter geometry[10] on the detector image plane is created based on postflight vehicle attitude data (Fig. 6) and the attitude of the telescope. Next, the Orbiter-geometry projection is scaled based on the known characteristics of the imaging system. From there, the edges of the Orbiter in the IR image frame are detected. This step was made difficult by the slightly blurred edges associated with image resolution, reduced signal due to possible dropoff of directional emissivity, and low signal on the Orbiter body flap as compared to background signal from the sky. To handle this, a gradient/thresholding process was used. Finally, the Orbiter-geometry projection is registered with the measured IR image by enclosing the edges of the two images in a rectangle and overlaying one on top of the other. The details of the complete process are given in Ref. 9. An example of the final result is given in Fig. 14, which shows the location of the eight thermocouples on the measured image. (Note that the size of the dots representing the thermocouples is enlarged for display purposes.)

Once the pixel locations of the thermocouples have been identified, the difference between the thermocouple and IR temperatures can be calculated for each frame. The temperature differences do not necessarily provide an absolute temperature measure because of flight thermocouple measurement uncertainties. Uncertainty estimates based on previous thermocouple Orbiter thermocouple sensor measurements[11] are about 1–2%, resulting in an inferred surface temperature error of about 5–10%. Thus, the question is, can

an independent calibrated temperature global IR image (without thermocouples) provide as good as flight temperature data as thermocouples?

Figure 15 shows the relative difference between the flight thermocouple temperatures and the ground calibrated IR temperatures. All temperature differences are less than about 5%, except for the thermocouple measurement near the elevon gap (number 850) that clearly shows a bias. A possible explanation for this bias is that the IR resolution ranges from about 3 to 6 in. at the image distances and the thermocouple measure at a point (essentially). Thus, with a sharp temperature gradient, as would exist at, or near, the elevon gap, the IR temperatures would tend to average to a different value. In general, however, the differences are less than about 5%, which lends credence that an independent calibrated global IR image (without thermocouples) can provide comparable flight temperature data. However, when thermocouple data are available, the preference would be to integrate these data into the data processing of the IR images to take full advantage of the thermocouple measurements. In general, thermocouple data can be used as a calibration source[9] or a validity check on the calibration and processing technique. The latter is what has been done in this report.

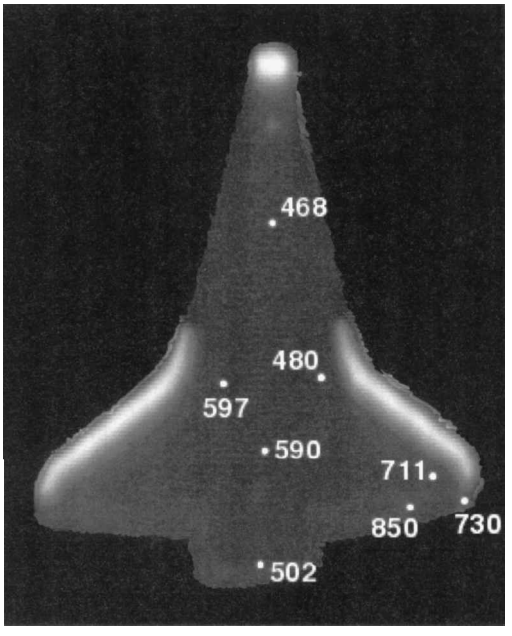

Fig. 14 Location of thermocouples on IR image.

Summary

An IR experiment is being developed as a general versatile tool to provide quantitative flight global heating data for reentry vehicles at hypervelocity speeds. The experiment is called ISAFE, and its primary goal is to identify, monitor, and quantify hypersonic boundary-layer transition for the X-33 vehicle during flight. This includes, specifically, the global mapping of the transition movement over the windward surface. The data collected during flight will serve as a calibration and validation of current boundary-layer transition prediction techniques. In addition, the flight experiment goal is to provide benchmark laminar, transitional, and fully turbulent global aeroheating data to validate existing wind-tunnel and computational results and to advance aeroheating technology.

The Shuttle Orbiter flights were selected as targets of opportunity to demonstrate the capability of the ground-based IR equipment and the data reduction techniques, to mitigate the aeroheating experimental risks before the first flight of the X-33. The shuttle serves as an ideal target to provide data for development of heating measurements and processing techniques because there is a vast aeroheating database that currently exists. Also, shuttle aeroheating flight data are collected during each reentry using surface thermocouples.

IR imagery was collected during the STS-96 landing at NASA KSC, Florida, on 6 June 1999. Presented are the first flight-test results in a series of flight tests to develop the IR technology for boundary-layer transition global mapping. Only two of the four basic ISAFE elements were chosen on the STS-96 flight. These were to mature the data acquisition (i.e., target acquisition, tracking, data recording, etc.) and the data reduction software to global temperatures. Both have been accomplished and the results presented.

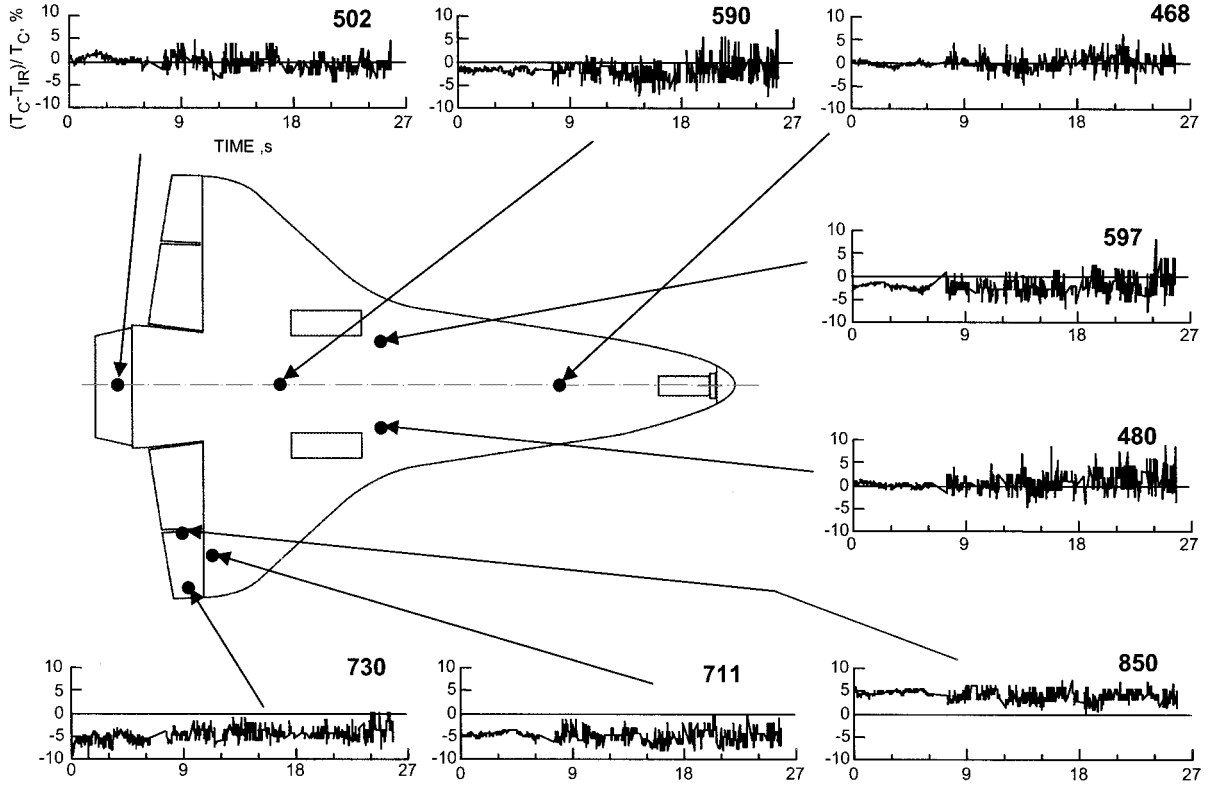

Fig. 15 Thermocouples and IR temperature differences for STS-96 ($t = 0$ is 1571.1 s from entry interface).

Calibrated radiance IR images were transformed to surface temperatures using a combination of ground calibrations and meteorology measurements taken at the time of the mission. To compare the IR derived temperatures with the thermocouple data, several image-processing techniques were developed. These techniques were applied to the IR images to find the thermocouple locations in the image to generate temperature differences. The differences between flight thermocouple and IR temperature data were generally less than about 5%, which is comparable to the expected accuracy of both types of aeroheating measurements. Thus, it has been shown that an independent calibrated temperature global IR image (without thermocouples) provides flight temperature data, comparable in accuracy to thermocouples.

Major accomplishments have been made with the data from the shuttle mission IR measurements, paving the way for a high probability of success for application to the X-33 flights. The work to date on the shuttle mission demonstrates the feasibility of applying the ground-based IR measurements and data reduction to the X-33 vehicle.

Acknowledgments

Conducting a flight experiment requires the talents of many people, who, behind the scenes, apply their skills in a professional and dedicated manner and contribute to the successful execution of the experiment. The authors acknowledge M. Lovern, Space and Naval Warfare Systems Center, San Diego, California, who is the overall manager of the Ballistic Missile Defense Organization (BMDO) Innovative Sciences and Technology Experimentation Facility (ISTEF) located at NASA Kennedy Space Center, that contains all of the mobile mount equipment and personnel used to acquire the infrared data; M. Monroe, Computer Sciences Corporation, Florida, who is the site manager of the BMDO/ISTEF; S. Welch, NASA Langley Research Center (LaRC), who is the ISAFE program manager; D. Levin, George Washington University (GWU), Washington, DC; R. Collins, GWU, Washington, DC, who provided consultation on the acquisition of the data; K. Sutton and H. Hamilton, NASA LaRC, who provided guidance in the heat transfer and boundary-layer phenomena; D. Banks, NASA Dryden Flight Research Center, who assisted in the formulation of the operational aspects of the experiment; and E. Hammer, NASA Headquarters, Houston, who provided considerable help with the shuttle trajectories. The authors express our appreciation to R. Wheless, NCI Information Systems, Inc., for the graphics assistance in the preparation of the paper.

References

[1] Berry, S. A., Horvath, T. J., Hollis, B. R., Thompson, R. A., and Hamilton, H. H., "X-33 Hypersonic Boundary-Layer Transition," AIAA Paper 99-3560, June 1999.

[2] Bouslog, S. A., An, M. Y., and Derry, S. M., "Orbiter Windward-Surface Boundary-Layer Transition Flight Data," edited by D. A. Throckmorton, NASA CP-3248, Pt. 2, 1995, pp. 703–739.

[3] Bertin, J. J., Hayden, T. E., and Goodrich, W. D., "Shuttle Boundary-Layer Transition Due to Distributed Roughness and Surface Cooling," *Journal of Spacecraft and Rockets*, Vol. 19, No. 5, 1982, pp. 389–396.

[4] Thompson, R. A., Hamilton, H. H., Berry, S. A., and Horvath, T. J., "Hypersonic Boundary-Layer Transition for X-33 Phase II Vehicle," AIAA Paper 98-0867, Jan. 1998.

[5] Horvath, T. J., Berry, S. A., Hollis, B. R., Liechty, D. S., Hamilton, H. H., and Merski, N. R., "X-33 Experimental Aeroheating at Mach 6 Using Phosphor Thermography," AIAA Paper 99-3558, June 1999.

[6] Hollis, B. R., Horvath, T. J., Berry, S. A., Hamilton, H. H., and Alter, S. J., "X-33 Computational Aeroheating Predictions and Comparisons with Experimental Data," AIAA Paper 99-3559, June 1999.

[7] Acharya, P. K., Robertson, D. C., and Berk, A., "Upgraded Line-of-Sight Geometry Package and Band Model Parameters for MODTRAN," Phillips Lab., TR PL-TR-93-2127, Geophysics Directorate, Hanscom AFB, MA, May 1993.

[8] Engelke, C. W., "LWIR Stellar Calibration: IR Spectral Curves for 30 Standard Stars," Lexington TR 908, Lincoln Labs., Massachusets Inst. of Technology, April 1991, Appendix B.

[9] Bozung, T. J., "Space Shuttle IR Image Calibration Using Thermocouple Data," M.S. Thesis, George Washington Univ. Joint Inst. for Advancement of Flight Sciences, Hampton, VA, March 2001.

[10] Weilmuenster, J. K., Gnoffo, P. A., and Greene, F. A., "Navier–Stokes Simulations of Orbiter Aerodynamic Characteristics," CP-3248, Pt. 1, NASA, edited by D. A. Throckmorton, 1995, pp. 447–494.

[11] Hartung, L. C., and Throckmorton, D. A., "Space Shuttle Entry Heating Data Book," Vol. 1-STS-2, NASA RP-1191, Pt. 1, May 1988.

I. E. Vas
Associate Editor

Color reproductions courtesy of NASA Langley Research Center.